RASĀYAN *J. Chem.*
Vol. 16 | No. 3 |1534-1542| July - September | 2023
ISSN: 0974-1496 | e-ISSN: 0976-0083 | CODEN: RJCABP
http://www.rasayanjournal.com
http://www.rasayanjournal.co.in

STRUCTURAL, QUANTUM CHEMICAL, AND MOLECULAR DOCKING INVESTIGATIONS OF A TRIAZOLE DERIVATIVE

R. Sharma[1], S. M. Deshmukh[2], S. Murugavel[3], D. Lakshmanan[4] and R. Kant[1,✉]

[1]Department of Physics, University of Jammu, Jammu Tawi-180006, (Jammu & Kashmir) India
[2]Department of Chemistry, Dr. B. R. Ambedkar National Institute of Technology, Jalandhar-144011, (Punjab) India.
[3]Department of Physics, Thanthai Periyar Government Institute of Technology, Vellore-632002, (Tamil Nadu) India
[4]Department of Physics, Thiruvalluvar University, Serkadu, Vellore-632115,(Tamil Nadu) India.
✉Corresponding Author: rkant.ju@gmail.com

ABSTRACT

The structure of a triazole derivative, (E)-4-((furan-2-ylmethylene)amino)-3-methyl-1H-1,2,4-triazole-5(4H)-thione (4FAMTT), has been elucidated using spectroscopic and single crystal X-ray diffraction studies. The crystal structure is stabilized by N2—H2···S1 intermolecular interaction that leads to the formation of a dimer. The computational investigations using Density Functional Theory (DFT) have been performed to optimize the geometrical parameters which, by and large, agree with the X-ray data. The Frontier Molecular Orbitals (FMOs) have been studied to estimate the kinetic stability and reactivity of the molecule. The global reactivity descriptors and molecular electrostatic potential (MEP) may help identify the molecule's reactive locations for possible interactions. The Hirshfeld surface (HS) and 2D fingerprint plot analysis have been employed to investigate inter-contacts in the crystal structure. The interaction energies that stabilize the crystal packing have been calculated and represented graphically. The molecular docking analysis indicates a high binding affinity of 4FAMTT for the COX-2 protein (PDB ID: 5KIR) and is able to bind its active site with a relatively strong interaction.

Keywords: X-ray Analysis, DFT, Hirshfeld Surfaces, Energy Frameworks, Molecular Docking.

RASĀYAN *J. Chem.*, Vol. 16, No. 3, 2023

INTRODUCTION

The triazole nucleus, one of the most important and well-known heterocycles, is an integral feature of a variety of natural products and medicinal agents.[1] It contains three nitrogen atoms in a five-membered ring having molecular formula $C_2H_3N_3$. Its nucleus forms the core structural component in the category of drugs, viz. antimicrobial, analgesic, anticonvulsant, antimalarial, antiviral, anticancer, and antioxidant activities.[2-9] Though many triazole-based derivatives are available as medicines, considerable attention has been received by the chemistry of triazoles and their fused heterocyclic derivatives because of their synthetic and effective biological importance.[10-14] Besides, a number of 1,2,4-triazole derivatives are commercialized as important fungicides, herbicides, and plant growth regulators.[15,16] The synthesis of (E)-4-((furan-2-ylmethylene)amino)-3-methyl-1H-1,2,4-triazole-5(4H)-thione (4FAMTT) has been carried out by using a standard process and the single crystals were obtained using slow evaporation technique. Its structural characterization has been carried out using various spectroscopic techniques and a fine description of the molecular structure has been realized using SCXRD. Since the X-ray structure of 4FAMTT exists in the literature, the present study primarily deals with quantum chemical and molecular docking investigations.[17] The DFT-based calculations have been performed to optimize the molecular structure and the global reactivity descriptors and complementary interaction sites in the structure have been identified using FMO and MEP mapping studies. The Hirshfeld surface analysis and the 3D topology of crystal packing have been discussed.

The molecular docking study helped explore the essential binding mode and possible interactions within the binding site of COX-2 protein (PDB ID: 5KIR).

http://doi.org/10.31788/RJC.2023.1638400

EXPERIMENTAL

Synthesis and Spectral Characterization

A mixture of N-amino-2-mercapto-5-methyl 1,3,4-triazole (0.01 mol) and furfural (0.01 mol) in methanol (15ml) to which 2 drops of glacial acetic acid were added and the same mixture heated on an oil bath for 4 hours, then concentrated and cooled. The separated solid was filtered and recrystallized from ethanol. The molecule synthesized as such is shown in Fig.-1(a). (E)-4-((furan-2-ylmethylene)amino)-3-methyl-1H-1,2,4-triazole-5(4H)-thione: Yield: 65%. M.p.: 250ºC. FT-IR (KBr, *v*, cm^{-1}): 3100-3200 broad (SH), 1620 (C=N), 1600 (C=C), 1070(-O-). ^{1}H NMR (DMSO-d6, ppm): 10.5(1H, singlet br, SH), 6.8-7.1(3H, m, aromatic protons), 2.1(1H, s, aromatic CH_3).

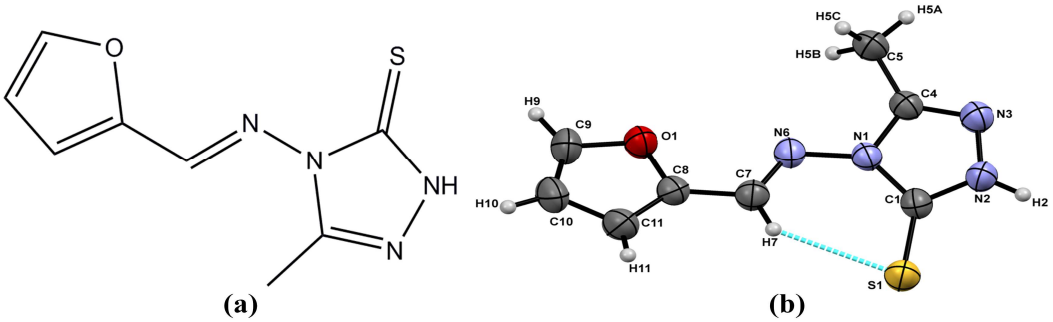

Fig.-1: (a) The Chemical Structure and (b) The X-ray Structure of 4FAMTT

Single Crystal XRD Studies

The single crystal X-ray diffraction study has been carried out by using a Rigaku Oxford Diffraction-make SCXRD equipped with MoKα radiation (wavelength = 0.71073Å). The intensity data collected have been reduced using the Olex 2 software.[18] The crystal structure has been solved by direct method using SHELXS-97 and refined by full-matrix least-squares on F^2 using SHELXL-97.[19,20] All hydrogen atoms were geometrically fixed. The non-H atoms were located from the E-map. A total of 159 parameters were refined with 1385 unique reflections. The final refinement yielded R=0.0455 (wR(F^2)= 0.1159), for all the data. The geometrical calculations have been performed using PLATON and PARST software.[21,22] The molecular and packing diagrams have been generated using the MERCURY software.[23] The SCXRD structure is shown in Fig.-1 (b) (ORTEP). The crystallographic data for the 4FAMTT structure are presented in Table-1.

Table-1: Crystallographic Data for $C_8H_8N_4OS$

CCDC number	2240398	Absorption coefficient	0.314 mm^{-1}
Empirical formula	$C_8H_8N_4OS$	F(000)	216
Formula weight	208.24	Theta range for data collection	3.82 to 26.37°
Temperature	293(2) K	Limiting indices	-5 ≤ h ≤ 5, -13 ≤ k ≤ 12, -13 ≤ l ≤ 13
Wavelength (MoKα)	0.71073 Å	Reflections collected / unique	5866 / 1385
Crystal system, space group	Triclinic, $P\bar{1}$	Data/restraints/ parameters	1385 / 0 / 159
Unit cell dimensions	a = 4.212(2) Å, α = 92.21(4)° b = 10.477(5) Å, β = 92.68(3)° c = 10.687(4) Å, γ = 90.19(4)°	Final R indices [I>2sigma(I)] R indices (all data)	R1 = 0.0669, wR2 = 0.1159 R1 = 0.0455, wR2 = 0. 0993
Volume Z	470.60(4) $Å^3$ 2	Largest diff. peak and hole	0.301 and -0.221 $eÅ^{-3}$
Calculated density	1.470 Mg/m^3	Goodness-of-fit on F^2	1.053

Computational Details

The molecular geometry optimization has been performed by DFT calculations using the Gaussian 09W software.[24] The atomic coordinates have been optimized in the ground state using the B3LYP method with a 6-311++G(d,p) basis set. Consequently, a reliable comparison of energy and other physiochemical

properties has been made. The resulting HOMO and LUMO energies have been used to find the chemical potential (μ), electronegativity (χ), electrophilicity index (ω) chemical hardness (η), and softness (S) of the molecule. The Crystal Explorer 21.5 software has been used to perform Hirshfeld surface investigations and fingerprint plots with interior and exterior distances (range from 0.4 Å to 3.0 Å) have also been generated.[25] Moreover, the intermolecular interaction energies and energy frameworks have been calculated. The molecular docking study has been performed using AutoDock Vina software, which predicts the binding affinity of small molecules to a protein.[26] The target protein used in the study is COX-2 (PDB ID: 5KIR), and it has been obtained from the Research Collaboratory for Structural Bioinformatics (RCSB) protein data bank.[27] The active site of the protein has been defined by setting the grid center for docking at the coordinates X = 22.901, Y = 1.684, and Z = 36.196. This allows the program to focus on the specific area of the protein where the compound is expected to bind. The docking study allows for the analysis of the entire ligand-protein interaction using the Discovery Studio 4.1 Visualizer software.[28]

RESULTS AND DISCUSSION

XRD Analysis

The molecule 4FAMTT ($C_8H_8N_4OS$) crystallizes in the triclinic space group $P\bar{1}$ with Z=2 and its unit cell molecular packing is shown in Fig.-2. Table-2 contains a few significant bond distances and angles. The dihedral angle between the planar triazole and the aromatic furyl ring is 14.2°. The S1—C1 distance of 1.667(2) Å indicates its double bond character.[29] The bond distances in the triazole ring match the literature values.[30] The torsion angle C1—N1—N6—C7 = 11.8° indicates that the furfurylidene group is rotated toward the viewer with respect to the triazole ring. A dimer with $R_2^2(8)$ a graph-set motif is formed due to the presence of N2—H2···S1 intermolecular interaction. The hydrogen bonding interactions and π···π interactions are given in Tables-3 and -4, respectively. The DFT calculations indicate that the values of the optimized geometry (bond lengths and bond angles) are comparable with the X-ray data.

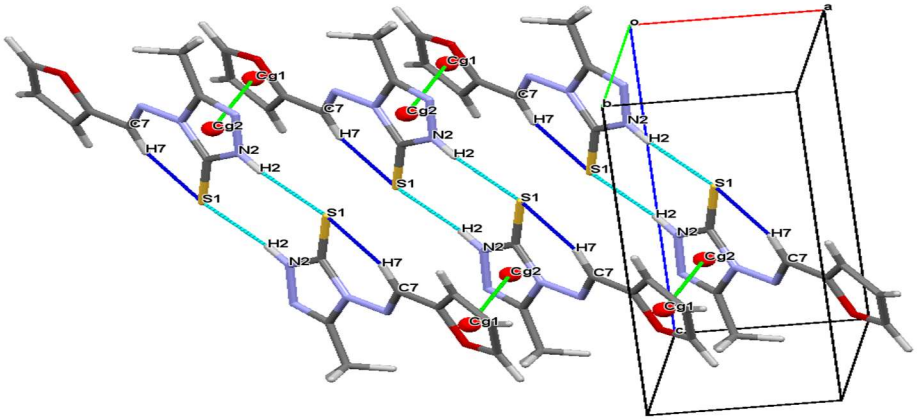

Fig.-2: Intermolecular Interactions and Packing View of the Crystal Structure.

Table-2: Selected Bond Lengths (Å) and Bond Angles (°)

Bond Lengths (Å)	XRD	DFT	Bond Angles (°)	XRD	DFT
C1—S1	1.667(2)	1.672	N1—C4—N3	110.8(2)	110.9
C1—N1	1.388(3)	1.402	N1—C4—C5	123.0(2)	123.6
C4—N1	1.382(3)	1.394	N3—C4—C5	126.2(2)	125.5
C4—N3	1.295(3)	1.297	S1—C1—N2	127.4(2)	126.4
N2—N3	1.371(3)	1.369	S1—C1—N1	130.6(2)	132.1
C1—N2	1.336(3)	1.357	C1—N1—C4	108.4(2)	108.2
C4—C5	1.472(3)	1.484	N1—N6—C7	119.4(2)	120.2
N1—N6	1.389(2)	1.371	N6—C7—C8	119.5(2)	118.9
C7—N6	1.272(3)	1.288	N6—N1—C4	118.1(2)	118.4
C7—C8	1.430(3)	1.440	N6—N1—C1	133.5(2)	133.3
C8—O1	1.359(3)	1.373	N2—N3—C4	104.0(2)	104.4
C9—O1	1.368(3)	1.354	C1—N2—N3	114.9(2)	115.0

C8—C11	1.348(3)	1.371	N1—C1—N2	102.0(2)	101.4
			C7—C8—O1	118.1(2)	115.5
			C7—C8—C11	132.5(2)	135.0
			C8—O1—C9	106.2(2)	107.2

Table-3: Hydrogen Bond Geometry (Å, °)

D – H···A	D – H	H···A	D···A	D – H···A
C7—H7···S1	0.91(3)	2.53(2)	3.219(3)	133.3(2)
N2—H2···S1^{i}	0.84(3)	2.50(3)	3.335(2)	170(3)

Symmetry code: i) 2-x,2-y,1-z

Table-4: Cg…Cg Interactions

CgI···CgJ	CgI···CgJ(Å)	CgI···P(Å)	α(°)	β(°)	Δ(Å)
Cg1···Cg2^{i}	4.6895(1)	3.423	14.16	49.61	10.27
Cg2···Cg1^{ii}	4.6895(1)	3.039	14.16	43.12	12.76

Symmetry code: i) -1+x, y, z ii) 1+x, y, z. Cg1 and Cg2 represents the centroid of (O1—C9) and (N1—C4) rings, respectively.

Frontier Molecular Orbitals

The energy gap between the highest occupied and lowest unoccupied orbitals is 3.78 eV. It predicts the kinetic stability (less) and reactivity (more) of the molecule.[31,32] The HOMO offers electrons for donation, whereas the LUMO accepts them. Moreover, the small energy gap explains the eventual charge transfer interactions taking place within the molecule. The energy level diagram is shown in Fig.-3. The molecular descriptors have been studied to investigate the chemical properties of the molecule (Table-5).

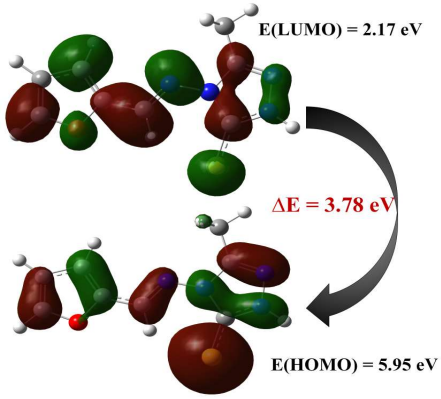

Fig.-3: HOMO-LUMO Energies of the 4FAMTT Molecule

Table-5: Global Reactivity Parameters using DFT Approach B3LYP/6-311++G(d, p) Basis Set

Property	Value
E_{HOMO}, E_{LUMO}	-5.95 eV, -2.17 eV
Orbital energy gap $E_g = (E_L - E_H)$	3.78 eV
Chemical hardness $\eta = (E_L - E_H)/2$	1.89 eV
Chemical potential $\mu = (E_L + E_H)/2$	-4.06 eV
Ionization potential ($-E_H$)	5.95 eV
Electron affinity ($-E_L$)	2.17 eV
Electronegativity ($\chi = -\mu$)	4.06 eV
Global softness ($\sigma = 1/2\eta$)	0.26 eV^{-1}

Molecular Electrostatic Potential and Mulliken Atomic Charges

The MEP and Mulliken charges and their manifestation in the form of surface maps are shown in Fig.-4. The MEP shows the possible nucleophilic and electrophilic (reactive) sites of the molecule. The yellow and blue color shows the electrophilic regions around the nitrogen (N3) and sulphur (S1) atoms and the high electropositive region around the —NH (Fig.-4(a)). The Mulliken charge distribution and its analysis (Fig.-4(b)) indicate that all the hydrogen atoms in the molecule have a positive charge. The positive

charges are located on N1, C1, C4, C5, C9, and C11 atoms, while the negative charge is on the remaining atoms. There exists a strong intermolecular N2—H2···S1 interaction.

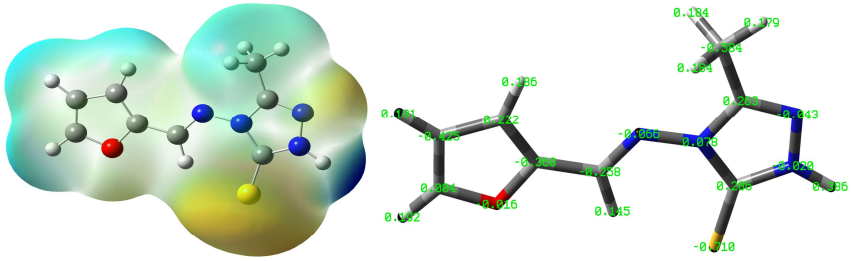

(a) (b)

Fig.-4: (a) Molecular Electrostatic Potential (MEP) and (b) Atomic Charges Computed by DFT Approach

Hirshfeld Surfaces and 2D Fingerprint Plot Analysis

The intermolecular interactions in the crystal structure are quantified using Hirshfeld surface analysis. This is a graphical tool for the visualization and understanding of intermolecular interactions.[25] The interconnects are highlighted by conventional mapping of d_{norm} on molecular Hirshfeld surfaces, as shown in Fig.-5(a). The red spots over the surface indicate the interconnects involved in the hydrogen bonds. In the shape index map (Fig.-5(b)), there are some red and blue triangles adjacent to each other which indicate the existence of weak π···π interactions. The curvedness map (Fig.-5(c)) shows the planar stacking present between the molecules as there are some flat patches on the surface of the molecule.

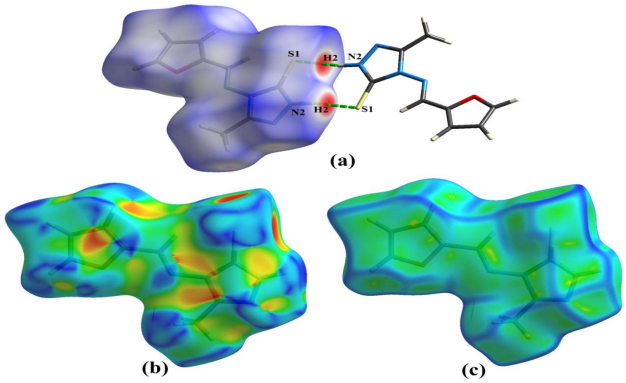

(a)

(b) (c)

Fig.-5: Hirshfeld Surface Analysis Mapped with (a) d_{norm} (b) Shape Index and (c) Curvedness Plot

The 2D fingerprint plots are given in Fig.-6. The dominant interactions with percentage contributions to the total HS are H···H (35.2%), S···H/H···S (18.4%), N···H/H···N (12.3%), C···H/H···C (11.5%) and others (O···H, C···C, N···C, N···N, N···O; 19.9%). The H···H inter contacts demonstrate large surfaces, whereas the N···H plot demonstrates the presence of N···H contact with the two characteristic wings. The S···H intercontacts with two narrow pointed wings support N—H···S non-classical hydrogen bonds. Furthermore, the C···H plot reveals information about the intermolecular hydrogen bonds.

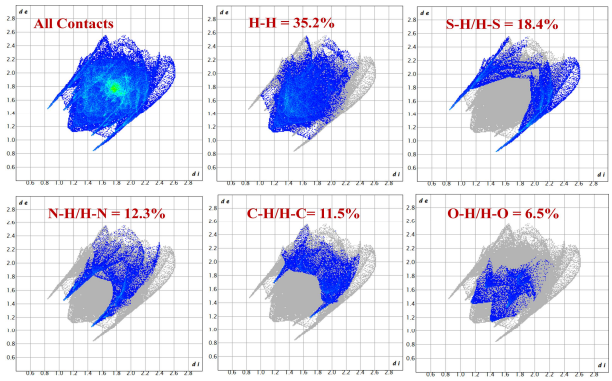

Fig.-6: 2D Fingerprint Plots Depicting the Relative Percentage Contribution to the HS Area for Various Contacts

Energy Framework Analysis

The energy framework calculations have been performed using the Crystal Explorer 21.5 software.[25] The symmetry operations were employed using the B3LYP/6-31G(d,p) functional basis set. The scaling factors used for benchmarked energies for B3LYP/6-31G(d,p) are k_{ele} = 1.015, k_{pol} = 0.740, k_{disp} = 0.871, and k_{rep} = 0.618.[33] In Table-6, the R represents the distance between the mean atomic positions (molecular centroids). The resulting interaction energies between the molecular pairs reveal that the electrostatic energy (-131.3 kJ/mol) dominates the dispersion energy (-30.0 kJ/mol). Figure-7 illustrates the visual representation of the molecular interaction energies when viewed along the b-axis.

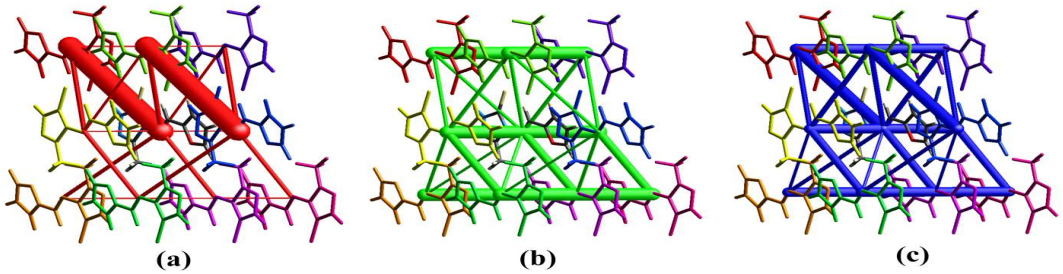

Fig.-7: Pictorial Representation of the (a) Coulomb Interaction Energy, (b) Dispersion Energy, and (c) Total Energy in Red, Green, and Blue Colors Along b-axis

Table-6: Different Molecular Interaction Energies (kJ/mol)

	N	Symop	R	Electron Density	E_ele	E_pol	E_dis	E_rep	E_tot
	1	-x, -y, -z	8.97	B3LYP/6-31G(d,p)	-64.9	-12.7	-12.9	81.0	-39.2
	0	-x, -y, -z	9.89	B3LYP/6-31G(d,p)	-11.9	-2.2	-9.9	14.7	-13.8
	1	x, y, z	4.21	B3LYP/6-31G(d,p)	-4.8	-1.9	-53.7	28.6	-35.6
	1	-x, -y, -z	6.86	B3LYP/6-31G(d,p)	-13.8	-3.1	-13.1	19.6	-16.2
	0	-x, -y, -z	7.07	B3LYP/6-31G(d,p)	-0.8	-0.4	-12.4	6.4	-8.1
	1	-x, -y, -z	7.70	B3LYP/6-31G(d,p)	-6.3	-2.9	-10.8	13.6	-9.8
	0	-x, -y, -z	8.51	B3LYP/6-31G(d,p)	-2.2	-0.5	-11.7	5.1	-9.7
	1	x, y, z	11.28	B3LYP/6-31G(d,p)	0.2	-0.2	-3.3	0.4	-2.5
	0	-x, -y, -z	7.82	B3LYP/6-31G(d,p)	-8.0	-2.1	-14.6	9.4	-16.9
	0	-x, -y, -z	7.74	B3LYP/6-31G(d,p)	-13.0	-3.6	-30.1	27.5	-25.6
	0	-x, -y, -z	10.26	B3LYP/6-31G(d,p)	-1.3	-0.4	-4.0	0.8	-4.7

Molecular Docking Analysis

The AutoDock Vina software has been used to study the interaction profile of 4FAMTT with the COX-2 (PDB ID: 5KIR) target protein.[26] COX-2 is an enzyme that is involved in the production of prostaglandins, the chemical mediators of inflammation and pain. It is over-expressed in certain diseases such as osteoarthritis, rheumatoid arthritis, and certain types of cancer. Therefore, developing specific COX-2 inhibitors can be useful to treat these diseases.[34,35] The binding pose of the 4FAMTT at the binding site of the 5KIR enzyme is shown in Fig.-8(a). It provides a visual representation of how the molecule is positioned at the active site of the protein. The two-dimensional (2D) binding interaction with the 5KIR binding site (Fig.-8(b)) illustrates the specific interaction between the molecule and the residues at the active site of the protein. The binding energy, distance, and bonding type of the molecule with the 5KIR enzyme (Table-7) provide quantitative information about the strength of the binding interactions and the distance between various atoms of the molecule and the protein. This piece of information helps

us understand the binding mechanism of the molecule and its potential as a drug candidate. The 4FAMTT - 5KIR complex is stabilized by multiple types of interactions. These include three conventional hydrogen bonds, two carbon-hydrogen bonds, and three hydrophobic interactions. The conventional hydrogen bonds occur between the donor hydrogen atom of the residue SER126 and GLN372 with the nitrogen and oxygen atom of the molecule at a distance of 2.27 Å and 2.51 Å. Further one more between the oxygen atom of the ILE124 and hydrogen atom of the molecule at a distance of 2.30 Å. This interaction is important for the compound to bind to the protein and helps to stabilize the complex. A carbon-hydrogen bond occurring between the donor hydrogen atoms of the residue ASP125 interacts with the nitrogen atom of the molecule at a distance of 2.69 Å. Similarly, a carbon-hydrogen bond occurs between LYS369 with the molecule at a distance of 3.39 Å. These interactions also contribute to the stability of the complex. The three hydrophobic interactions involve the non-polar atoms of the compound and the protein and help bury the molecule into the protein surface, which further stabilizes the complex. The hydrophobic interaction (π-π T-shaped) exists between 4FAMTT and protein TYR373 at a distance of 4.97Å. Also, the alkyl hydrophobic interaction occurs between the carbon of the molecule with ALA543 and PRO542 at a distance of 4.05 Å and 3.86 Å, respectively. A binding energy score of -6.5 Kcal/mol for the 4FAMTT - 5KIR complex confirms that the molecule is able to bind to the protein with a relatively high binding affinity, which is a good indication that it will act as a potent inhibitor for COX-2.

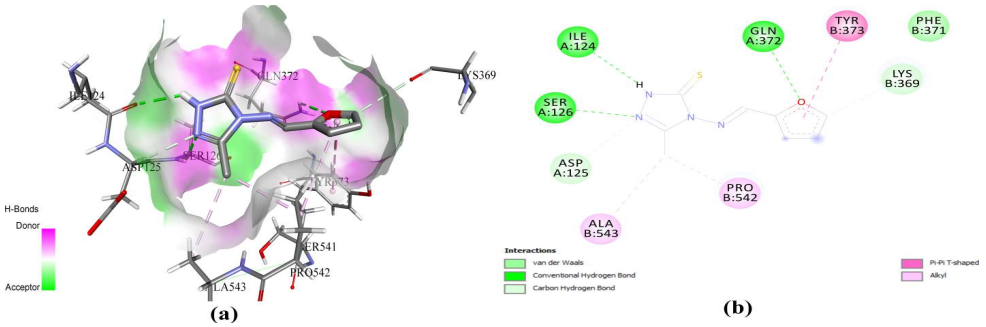

Fig.-8: (a) Molecular Binding Interaction of 4FAMTT to 5KIR Binding Site and (b) The 2D Binding Interaction of 4FAMTT to 5KIR Binding Site

Table-7: Binding Energy, Hydrogen Bond, Electrostatic and Hydrophobic Contacts of (E)-4-((furan-2-ylmethylene)amino)-3-methyl-1H-1,2,4-triazole-5(4H)-thione to 5KIR

Inhibitor	Binding Energy (Kcal mol^{-1})	Interactions	Distance Å	Bonding	Bonding Types
4FAMTT	-6.5	SER126[H….N]	2.27	Hydrogen Bond	Conventional
		GLN372[H….O]	2.51	Hydrogen Bond	Conventional
		ILE124 [O....H]	2.30	Hydrogen Bond	Conventional
		ASP125[H....N]	2.69	Hydrogen Bond	Carbon H-bond
		LYS369[O....C]	3.39	Hydrogen Bond	Carbon H-Bond
		TYR373 [π.... π]	4.97	Hydrophobic	π – π T-Shaped
		ALA543 [π.....C]	4.05	Hydrophobic	Alkyl
		PRO542 [π.....C]	3.86	Hydrophobic	Alkyl

CONCLUSION

The molecule, 4FAMTT, crystallizes in the triclinic crystal system having $P\bar{1}$ space group. The theoretically determined values of the bond distances and angles are in close proximity to the X-ray measurements. The N2—H2···S1 interaction yields a dimer having $R_2^2(8)$ a graph-set motif. The energy gap between the FMO is 3.78 eV, which implies the stability of the molecule. The charge distribution on the MEP map shows the chemical reactivity sites of the molecule. The Hirshfeld surface analysis revealed the N-H···S intermolecular interactions in the crystal. The 2D Fingerprint plots represent that the major contribution comes from H···H (35.2%) contacts. The construction of energy frameworks indicates that the electrostatic energy is dominant over the dispersion energy. The resulting analysis of the molecular docking study with the 4FAMTT and the 5KIR enzyme shows a very good binding energy of -6.5

kcal/mol. This value confirms that 4FAMTT has a high binding affinity for the protein and is able to bind to the active site of the enzyme with a relatively strong interaction.

ACKNOWLEDGMENTS

The corresponding author is thankful to scientific agencies like DST, ICMR, CSIR, and UGC for having funded the crystallography research at the University of Jammu during the past three decades.

CONFLICT OF INTERESTS

The authors declare that there is no conflict of interest.

AUTHOR CONTRIBUTIONS

All the authors contributed significantly to this manuscript, participated in reviewing/editing, and approved the final draft for publication. The research profile of the authors can be verified from their ORCID ids, given below:

R. Sharma https://orcid.org/0000-0002-5698-4067
S.M. Deshmukh https://orcid.org/0000-0002-7913-7952
S. Murugavel https://orcid.org/0000-0002-4626-8104
D. Lakshmanan https://orcid.org/0000-0002-7672-2689
R. Kant https://orcid.org/0000-0001-8043-2329

REFERENCES

1. R. Kharb, P. C. Sharma and Mohd S. Yar, *Journal of Enzyme Inhibition and Medicinal Chemistry*, **26,** 1(2011), https://doi.org/10.3109/14756360903524304
2. K. Kushwaha, N. Kaushik and S. C. Jain, *Bioorganic and Medicinal Chemistry,* **24(7),** 1795(2014), https://doi.org/10.1016/j.bmcl.2014.02.027
3. H. N. Hafez, H. A. Abbas and A. R El-Gazzar, *Acta Pharm*aceutica, **58**, 359(2008), https://doi.org/10.2478/v10007-008-0024-1
4. L. P. Guan, Q. H. Jin, G. R. Tian, K. Y. Chai and Z. S. Quan, *Journal of Pharmaceutical Sciences*, **10,** 254(2007)
5. R. Gujjar, A. Marwaha, J. White, L. White, S. Creason, D. M. Shackleford, J. Baldwin, W. N. Charman, F. S. Buckner, S. Charman, P. K. Rathod and M. A. Phillips, *Journal of medicinal chemistry*, **52,** 1864(2009), https://doi.org/10.1021/jm801343r
6. B. A. Johns, J. G. Weatherhead, S. H. Allen, J. B. Thompson, E. P. Garvey, S. A. Foster, J. L. Jeffrey and W. H. Miller, *Bioorganic and Medicinal Chemistry Letters,* **19,** 1802(2009), https://doi.org/10.1016/j.bmcl.2009.01.090
7. A. Duran, H. N. Dogan and S. Rollas, *IL Farmaco,* **57,** 559(2002), https://doi.org/10.1016/S0014-827X(02)01248-X
8. D. Verbanac, R. Malik, M. Chand, K. Kushwaha, M. Vashist, M. Matijasic and S. C. Jain, *Journal of Enzyme Inhibition and Medicinal Chemistry,* **31**, 104(2016), https://doi.org/10.1080/14756366.2016.1190714
9. S. Kumar, S. L. Khokra, and A. Yadav, *Future Journal of Pharmaceutical Sciences,* **7**, 106(2021), https://doi.org/10.1186/s43094-021-00241-3
10. K. Sztanke, T. Tuzimski and J. Rzymowska, *European journal of medicinal chemistry,* **43,** 404(2008), https://doi.org/10.1016/j.ejmech.2007.03.033
11. M. Palko, M. El Haimer, Z. Kormanyos and F. Fulop, *Molecules,* **24(4),** 772(2019), https://doi.org/10.3390/molecules24040772

12. M. J. Vaishnani and V. D. Jain, *Rasayan Journal of Chemistry*, **16(2),** 811(2023), http://doi.org/10.31788/RJC.2023.1628271
13. N. Depa and H. Erothu, *Rasayan Journal of Chemistry,* **15(3),** 1709(2022), http://doi.org/10.31788/RJC.2022.1536924
14. M. R. Archana, K. H. Shivaprasad and K. G. Shilpa, *Rasayan Journal of Chemistry,* **14(4)**, 2652(2021), http://dx.doi.org/10.31788/RJC.2021.1446506
15. J. He, L. Feng, J. Li, R. Tao, F. Wang, X. Liao, Q. Sun, Q. Long, Y. Ren, J. Wan, *Bioorganic and Medicinal Chemistry*, **20**, 1665(2012), https://doi.org/10.1016/j.bmc.2012.01.019
16. K. Oh, K. Yamada, T. Asami and Y. Yoshizawa, *Bioorganic and Medicinal Chemistry Letters,* **22**, 1625(2012), https://doi.org/10.1016/j.bmcl.2011.12.120
17. A. K. Sen, R. N. Singh, R. N. Handa, S. N. Dubey, P. J. Squattrito, *Journal of Molecular Structure*, **470**, 61(1998), https://doi.org/10.1016/S0022-2860(98)00470-0
18. O. V. Dolomanov, L. J. Bourhis, R. J. Gildea, J. A. Howard and H. Puschmann, *Journal of applied crystallography,* **42**, 339(2009), https://doi.org/10.1107/S0021889808042726
19. G. M. Sheldrick, *Acta Crystallographica Section A: Foundations and Advances,* **64**, 112(2008), https://doi.org/10.1107/S0108767307043930
20. G. M. Sheldrick,*Acta Crystallographica,* **C71,** 3(2015), https://doi.org/10.1107/S20532733140263 70
21. A. L. Spek, *Acta Crystallographica Section D: Structural Biology,* **65**, 148(2009), https://doi.org/10.1107/S090744490804362X
22. M. Nardelli, *Computers & Chemistry*, **7,** 95(1983), https://doi.org/10.1107/S0021889895007138
23. C. F. Macrae, I. J. Bruno, J. A. Chisholm, P. R. Edgington, P. McCabe, E. Pidcock, L. Rodriguez-Monge, R. Taylor, J. V. Streek and P. A. Wood, *Journal of applied crystallography,* **41**, 466(2008), https://doi.org/10.1107/S0021889807067908
24. A. Frisch, *Gaussian 09W Reference*, (Wallingford, USA, 2009) p. 25
25. P. R. Spackman, M. J. Turner, J. J. McKinnon, S. K. Wolff, D. J. Grimwood, D. Jayatilaka and M. A. Spackman, *Journal of applied crystallography,* **54,** 1006(2021), https://doi.org/10.1107/S1600576721002910
26. G. M. Morris, R. Huey, W. Lindstrom, M. F. Sanner, R. K. Belew, D. S. Goodsell and A. J. Olson, *Journal of computational chemistry,* **30(16),** 2785(2009), https://doi.org/10.1002/jcc.21256
27. https://www.rcsb.org
28. BIOVIA discovery studio visualizer, Software version, **20**, 779(2016).
29. J. L. Escobar-Valderrama, J. H. Garcia-Tapia, J. Ramirez-Ortiz, M. J. Rosales, R. A. Toscano and J. Valdes-Martinez, *Canadian journal of chemistry,* **67,** 198(1989), https://doi.org/10.1139/v89-033
30. M. Ghassemzadeh, M. Tabatabaee, S. Soleimani, B. Neumuller, *Zeitschrift fur anorganische und allgemeine Chemie,* **631,** 1871(2005), https://doi.org/10.1002/zaac.200500140
31. P. Akhileshwari, K. R. Kiran, M. A. Sridhar, M. P. Sadashiva, and N. K. J. Lokanath, *Journal of Molecular Structure,* **1242,** 130747(2021), https://doi.org/10.1016/j.molstruc.2021.130747
32. A. Bendjeddou, T. Abbaz, A. Ayari, M. Benahmed, A. Gouasmia, and D. Villemin, *Oriental journal of chemistry,* **32 (2),** 799(2016), https://doi.org/10.13005/ojc/320205
33. A. J. Edwards, C. F. Mackenzie, P. R. Spackman, D. Jayatilaka and M. A. Spackman, *Faraday Discussions,* **203** 93(2017), https://doi.org/10.1039/C7FD00072C
34. M. O. E. Hilario, M. T. Terreri and C. A. Len, *Jornal de pediatria (Rio J)*, **82(8),** 206(2006), https://doi.org/10.2223/JPED.1560
35. E. Ricciotti and G. A. FitzGerald, *Arteriosclerosis, Thrombosis, and Vascular Biology,* **31(5),** 986(2011), https://doi.org/10.1161/ATVBAHA.110.207449

[RJC- 8400/2023]